

Article

Effects of Red Mud Leachate on the Microstructure of Fly Ash-Modified Red Clay Anti-Seepage Layer under Permeation

Yibo Zhang ^{1,*} , Yulong Wang ¹, Yue Yu ¹, Hongkang Hu ¹, Hao Qin ¹ and Daoping Peng ²¹ School of Emergency Management, Xihua University, Chengdu 610039, China; qinhao@stu.xhu.edu.cn (H.Q.)² Faculty of Geosciences and Environmental Engineering, Southwest Jiaotong University, Chengdu 611756, China; pdp0330@swjtu.edu.cn

* Correspondence: yibo@mail.xhu.edu.cn

Abstract: In recent years, the ecological safety issues of red mud tailings ponds have been frequent, with problems such as the seepage damage of anti-seepage materials at the bottom of tailings ponds, failure of anti-seepage systems, and leakage of pollutants. In order to deeply analyze the influence of red mud (RM) leachate on the microstructure of the modified red clay (RC) anti-seepage layer, this article explores the influence characteristics of strong alkaline RM leachate on the microstructure of a modified RC anti-seepage layer under actual working conditions through a combination of permeability tests and microscopic characterization. The results showed that as the RM leachate permeation time increased, varying changes occurred in the permeability coefficient of the modified RC with different FA contents, among which the permeability coefficient of the modified RC with an 8% FA content showed a significant decreasing trend, reaching 5.98×10^{-11} m/s after stabilization. After permeation, numerous small pores were generated in the modified clay; furthermore, the small particles of the FA-modified clay were significantly reduced compared to pure clay. As the permeation time increased, the 8% FA-modified RC showed a phenomenon of first increasing and then decreasing in specific surface area, with a small change from 27.71 m²/g to 27.52 m²/g, indicating that this sample had high stability and the specific surface area was not significantly affected by permeation. This is mainly caused by the influence of gelling materials produced by the pozzolanic reaction and activation effect upon FA addition. The soil structure became more compact at the microscopic level with increasing FA content, resulting in particle aggregation, increased specific surface area, and narrowed small-pore size distribution. After 60 days of permeation, the single-shoulder peak of the 8% FA-modified RC was still the lowest at about 0.30 dV/dr. Compared to other samples, the pore size was smaller and less affected by the leachate. Overall, the microstructure of the 8% FA-modified RC was less affected by the leachate. This study provides an explanatory basis for the macroscopic mechanical phenomena by analyzing the influence of microstructure. It further provides a reference for studying the selection of anti-seepage materials.



check for updates

Citation: Zhang, Y.; Wang, Y.; Yu, Y.; Hu, H.; Qin, H.; Peng, D. Effects of Red Mud Leachate on the Microstructure of Fly Ash-Modified Red Clay Anti-Seepage Layer under Permeation. *Sustainability* **2023**, *15*, 15161. <https://doi.org/10.3390/su152015161>

Academic Editor: Marco Lezzerini

Received: 30 August 2023

Revised: 14 October 2023

Accepted: 17 October 2023

Published: 23 October 2023

Keywords: modified red clay; red mud leachate; microstructure; adsorption characteristics; permeation time

1. Introduction

Tailings are mining components with low useful content and are currently unusable for industrial production purposes, thereby constituting a significant component of industrial solid waste [1]. Recently, tailings-related safety issues have become an increasingly important cause for concern, whereby the leakage of pollutants and destruction of anti-seepage materials—which lead to the failure of the anti-seepage system—have become hot topics of research regarding efforts to ensure the safety of the external ecological environment of tailing ponds [2,3]. Red mud (RM) is an industrial solid waste consisting of very fine mud particles produced in the process of bauxite production of alumina, which possesses high alkalinity and a high salt content and contains heavy metals. Currently, the tailing pond



Copyright: © 2023 by the authors. Licensee MDPI, Basel, Switzerland. This article is an open access article distributed under the terms and conditions of the Creative Commons Attribution (CC BY) license (<https://creativecommons.org/licenses/by/4.0/>).

storage method is primarily used for RM disposal [4]. By 2020, the cumulative stock of RM in the world had exceeded 2.7 billion, which not only occupies a large amount of land and wastes resources, but also may cause serious environmental pollution and safety hazards [5]. According to the 2021 Central Inspection Report [6], an aluminum company located in southwestern China experienced a phenomenon of RM permeation and leakage testing in a RM reservoir in 2013, which had a significant impact on the ecological environment. However, highly alkaline RM leachate will have a salinization effect on the foundation clay layer of the RM tailing pond, which can change the structure and chemical composition of the clay layer, thereby affecting its strength as well as the safety and stability of the tailing pond [7,8]. Given that most RM tailing ponds currently rely on clay anti-seepage layer materials, it is necessary to characterize the effect of RM leachate on the microstructure of the modified clay anti-seepage layer to ensure the safe operation of RM tailing ponds, which can provide theoretical support for the improvement of clay anti-seepage layers.

As clay, which is the main component of a compacted clay liner (CCL) system, has a large specific surface area, a high cation exchange capacity, and a very strong hydrophilicity, it can cause some pollutants present in the leachate to be retained in the anti-seepage layer. For example, suspended solids and metal ions can adhere to the pore space of the clay through the sedimentation effect [9,10], thus playing a dual role as both a chemical and a hydraulic barrier [11]. However, in practical engineering applications, clay properties are often changed by introducing different additives to enhance their anti-seepage properties. Sophia and Swaminathan [12] studied the electrolysis and stabilization of sludge by doping FA and cement. They found that doping with these two substances resulted in a substantial reduction in the leaching of chromium ions. In turn, Paramasivam et al. [13] mixed FA and sludge into clay of different densities to make 30 cm high soil columns by molds, which were then soaked with heavy metal-ion solutions. Their results showed that the clay of medium density was able to indirectly influence the leaching and downward transport of various elements, thus demonstrating a higher capacity to block heavy metals (except for lead). Similarly, Jeyaseelan and Qing [14] and Zhang et al. [15] used sludge ash and alkaline tailing materials to create modified soil using a certain blending ratio for ecological restoration. Their results showed that the soil samples blended with sludge, and ash had a positive effect on the reduction of their cadmium and lead contents. Furthermore, Metelková et al. [16] altered the pore size and, hence, the permeability coefficient of clay by adding CaO, and the pore size of the clay continued to decrease over the 360-day maintenance period with a CaO content of 4–8%, whereas it did not change at a 1% CaO content.

When leachate is transported in the clay anti-seepage system, the interaction between the leachate and the geotechnical medium leads to changes in the microstructure of the material, such as porosity and media properties, which directly affect the permeability of the material to the leachate [17–20]. Thus, for example, in a study of waste leachate-induced structural changes in clay, Oztoprak et al. [21] found that leachate effectively separated illite from clay by cation exchange, leading to structural disintegration, the formation of flocculated particle arrangements, and a reduction in clay strength. Additionally, through column tests, Guo et al. [22] found that when leachate flow rate was low, the leachate and clay mainly underwent a chemical reaction whereby some alkaline pollutants in the clay were dissolved, consequently reducing the extent of soil particle cementation, clay strength, and clay ability to resist deformation. In order to further understand the mechanism of clay structural changes under leachate action, many researchers have conducted micro-characterization and adsorption tests to study the micro-mechanisms at play. As a case in point, Ural et al. [23] showed that unexplained clay macroscopic physical or mechanical behavior can be elucidated using scanning electron microscopy (SEM) to examine the microstructure of clay particles and additives. Further, Zhang et al. [24] demonstrated the law of pore structure changes after the adsorption of the heavy metal Cd(II) by modified clay through an adsorption test. The results showed that the ideal maximum adsorption amount of Cd(II) by modified clay increased markedly, and the incorporation of an appropriate amount of sludge ash had a positive effect on the improvement of the specific surface areas.

Consistently, Zhao et al. [25] conducted microstructural and mechanical tests on compacted clay contaminated by waste leachate and showed that leachate contamination led to a decrease in the montmorillonite content of compacted clay, which disrupted the aggregate structure and caused an increase in the relative porosity of the smaller pores.

In summary, many researchers have studied the influence of leachate on the microstructure of the clay anti-seepage layer using experimental and characterization methods. However, most of them have focused on the waste leachate, whereas few have studied the strong alkaline RM leachate. Therefore, to further analyze the influence of highly alkaline RM leachate on the microstructure of a modified clay anti-seepage layer with different fly ash (FA) contents, we combined a permeability test with microscopic characterization under actual permeation conditions. The objective of this study is to analyze the effect of RM leachate on the microstructural changes of FA-modified clay through permeation in order to obtain the least affected modified clay. This study could provide an explanatory basis for the macroscopic mechanical phenomena by analyzing the influence of microstructure and further provide a reference for studying the selection of anti-seepage materials.

2. Materials and Methods

2.1. RC and FA Properties

The clay used in this study is a type of red clay (RC) found around a RM tailing pond in southwest China. A soil sample of 1 m below the ground surface was collected, loaded into high-density HDPE sampling barrels, sealed, and transported back to the laboratory for relevant tests. FA was collected from a power plant in Chengdu, China. The specific testing methods and results description of RC are detailed in our previous research [26]. The properties of RC and FA are listed in Table 1.

Table 1. Properties of RC and FA.

Physical Properties of RC									
Liquid Limit (%)	Plastic Limit (%)	Plasticity Index (%)	Initial Moisture Content (%)	Optimum Moisture Content (%)	Maximum Dry Density (g/cm ³)	Specific Gravity (Gs)	Compression Index (Cc)	Swelling Index (Cs)	
46.1	29.8	16.3	13.55	24	1.64	2.71	0.05	0.024	
Chemical composition (%)									
Constituent	SiO ₂	Al ₂ O ₃	Fe ₂ O ₃	CaO	Na ₂ O	MgO	K ₂ O	Others	
RC	55.96	26.16	6.37	0.06	0.12	0.66	1.0	9.66	
FA	49.40	28.87	5.8	3.49	0.90	0.78	2.43	8.32	

2.2. Leachate Properties

The RM leachate used in the test was collected from the drainage pipe of a RM tailing pond in southwest China. Various parameters, including pH, electric conductivity (EC), and oxidation-reduction potential (ORP), of the leachate samples were measured immediately after sampling. A portable multifunctional (pH-ORP-EC-TDS-DO) water quality detector (Model SD150D, Beijing Starwood Technology Co., LTD., Beijing, China) was used to test the parameters of the leachate. The leachate sample was sealed in an HDPE sample bottle and brought back to the laboratory for testing. Please refer to our previous research for the specific testing method and result description of the leachate [26]. Hydrochemical parameters and elemental composition of the RM leachate are summarized in Table 2.

Table 2. Hydrochemical parameters and elemental composition of RM leachate.

pH	EC@25 °C/mS-cm ⁻¹	ORP /mV	Ionic Strength /mM	Elemental Composition (mg·L ⁻¹)											
				Al	Ca	Na	Mg	K	Si	Cl ⁻	F ⁻	NO ₂	SO ₄ ²⁻	Cr	Cr (VI)
12.6	51.1	-110.0	484.3	745.5	57.1	10650	10.5	81.8	89.9	6490.5	121.8	483.4	7453.3	5.9	1.76

2.3. Sample Preparation and Permeability Test

For the purposes of this experimental work, five types of modified RC samples were designed with FA contents of 0% (pure RC), 2%, 4%, 6%, and 8%. RC samples were passed through a 5 mm sieve and mixed with FA in the specified proportion, after which the test samples were compacted at optimum moisture content and 95% of their maximum dry weight. The permeability test was conducted using a flexible wall infiltrometer. Sample preparation and test setup are shown in Figure 1.

**Figure 1.** Sample preparation and permeability testing device.

In the permeation process, the designed fixed effective perimeter pressure was 24.0 kPa, and the inflow-head RM leachate was 160 cm to simulate the actual permeability of the bottom of the RM tailing pond.

2.4. Characterization by SEM

In order to visually compare the changes in the microscopic pore structure of RC before and after FA modification, SEM was used to analyze the morphologies of the representative 0%, 4%, and 8% FA-modified RC samples, for which purpose these were air-dried prior to the preparation of the clay cross-sections through scissor cutting. The samples were produced into a block with length, width, and thickness all less than 1 cm and a mass of less than 200 g. Samples were then fixed on the stage with conductive adhesive and scanned by a SEM instrument, FEI Inspect F50, USA. The 100 μ m scale images were used for comparison of the modified RC with different FA contents, with 10.00 kV HV, 1000 \times mag, 9.9 mm WD, SE mode, ETD det. The 10 μ m scale images were used for comparison of the modified RC before and after the permeability test, with 10.00 kV HV, 10,000 \times mag, 10.0 mm WD, SE mode, ETD det.

In order to observe the electron microscope scanning images of the modified RC before and after permeation more intuitively, digital image processing technology was used for processing [27]. Firstly, the image is contrast-enhanced to improve its clarity and visual

effect, aiming to transform the image into a state that is easier to process and analyze. Then, the image is binarized using two color components black and white to represent the image, resulting in a pixel value of 0 (all black) and a pixel value of 255 (all-white image). After denoising, a smooth binary image is obtained.

2.5. BET Pore Analysis

The principle underlying the gas adsorption method to determine the specific surface area of a material is based on the adsorption characteristics of gases on solid surfaces. Specifically, the surface of the measured sample particle (adsorbent) has a reversible physical adsorption effect on the gas molecule (adsorbate) at ultra-low temperatures under any particular pressure. Further, there is a certain equilibrium adsorption amount corresponding to any given pressure [27]. Hence, by determining this equilibrium adsorption amount, the specific surface area of the sample can be equivalently calculated using a theoretical model.

In this work, the BET pore analyzer (Micromeritics ASAP 2460, Norcross, GA, USA) was used to determine the surface area of the modified RC. The experimental setup parameters include 77.350 K analysis bath temp, 10 s equilibration interval, none low pressure dose, no automatic degas, and 1.000 g/cm³ sample density.

The BET theoretical [28] calculations are based on the multilayer adsorption equation derived from the classical statistical theory by Brunauer, Emmett, and Teller to obtain the monolayer adsorption amount (V_m , Formula (1)) and calculate the specific surface area:

$$\frac{P}{V(P_0 - P)} = \frac{1}{V_m C} + \frac{(C - 1)}{V_m C} \times \frac{P}{P_0} \quad (1)$$

where V is the total volume of adsorbed gas at equilibrium pressure = P ; V_m is the volume of gas required to cover the catalyst surface with the first full layer; P is pressure of the adsorbed gas at equilibrium at the adsorption temperature; P_0 is the saturated vapor pressure; and C is the absorption-related constant.

3. Results and Discussion

3.1. Permeability Characteristics of Modified RC under RM Leachate

3.1.1. Permeability Behavior of Modified RC

The value of the permeability coefficient of the RC anti-seepage layer is an important indicator of the anti-seepage performance of the clay liner, which will change under the long-term corrosion of RM leachate [29]. The variation in the value of the permeability coefficients of the different FA-modified RC corroded by RM leachate is shown in Figure 2. In the early stage of the permeability test, the value of the permeability coefficient of the compacted modified RC increased with increasing FA content, while at the later stage of the test, it varied with FA content. In particular, the permeability coefficient for the 8% FA-modified RC stabilized at 5.98×10^{-11} m/s, which is smaller than the corresponding values for the 4% or 6% FA-modified RC, showing a relatively downward trend. It indicates that the 8% FA-modified RC is significantly affected by permeability, but its anti-seepage ability is enhanced. However, pure RC with a 0% FA content showed the smallest permeability coefficient, with a value of 9.87×10^{-12} m/s.

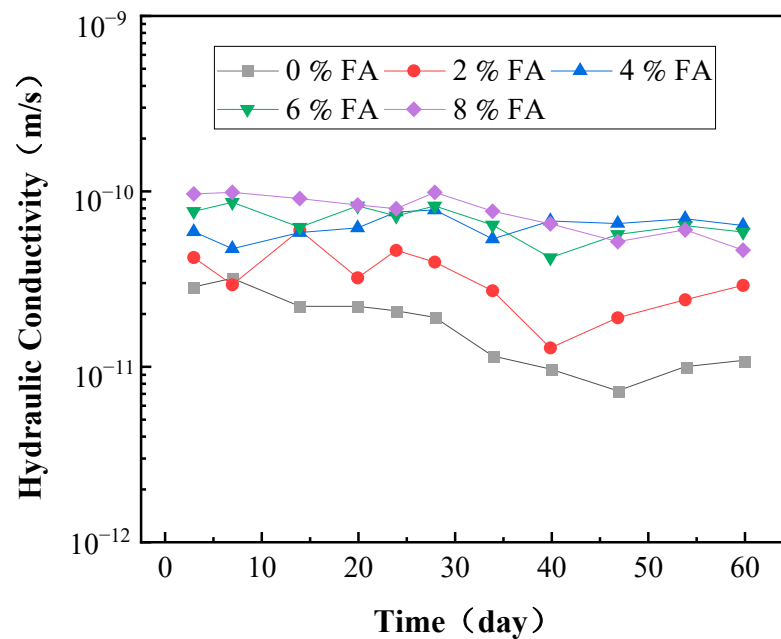


Figure 2. Permeability coefficient of modified RC with different FA contents after RM leachate corrosion.

3.1.2. Cause Analysis

The incorporation of FA into clay induces a short-term hydrolysis reaction and a long-term pozzolanic reaction [30]. In the early stage of the permeability test, the hydrolysis reaction mainly occurred between FA and the RC, whereby the CaO and MgO contained in the FA became rapidly hydrolyzed to produce a large number of free Ca^{2+} and Mg^{2+} cations. The RC surface is negatively charged; hence, the electrostatic attraction between cations became stronger as their valence increased, causing the concentration of the high-valence cations to rise, the diffusion layer to become increasingly thinner, and the internal structure of the RC to become more compact and stable. In turn, in the later stages of the permeability test, FA activity was enhanced due to the alkaline environment induced by RM leachate permeation [31]. As permeation time increased, FA reacted with the active minerals in the soil, including SiO_2 and Al_2O_3 , producing calcium silicate hydrates (CSH) and calcium aluminate hydrates (CAH). The crystals formed from the pozzolanic reaction and CAH acted together on the soil particles and the recycled fine aggregate particles to strengthen the overall structure of the soil through continual interaction, thus resulting in a stronger and more water-stable soil. This effect can become more pronounced with time [32]. In addition, the slow pozzolanic reaction of FA causes the pore size within the clay to become progressively smaller, whereas a compacted modified RC with a high FA content has a lower permeability coefficient because more pores are involved in the bonding with more FA, and less permeation of the RM leachate occurs [33].

3.2. Effects of RM Leachate on Modified RC Micro Particles

3.2.1. Comparative Analysis of SEM Results

Images from SEM observations of the modified RC with different FA contents are shown in Figure 3. Compared to pure clay, the 4% and 8% FA-modified RC showed a more compact structure, better connectivity, and a smoother surface, indicating a high level of reinforcement of the clay pore structure by FA. Meanwhile, in the RC with 4% and 8% FA contents, it was evident that granular material was tightly bound in the clay, particularly in the case of the 8% FA-modified RC. The microscopic morphology of FA showed the presence of a large number of glass beads, which were sufficiently filled in the pore structure of the clay after maintenance [34].

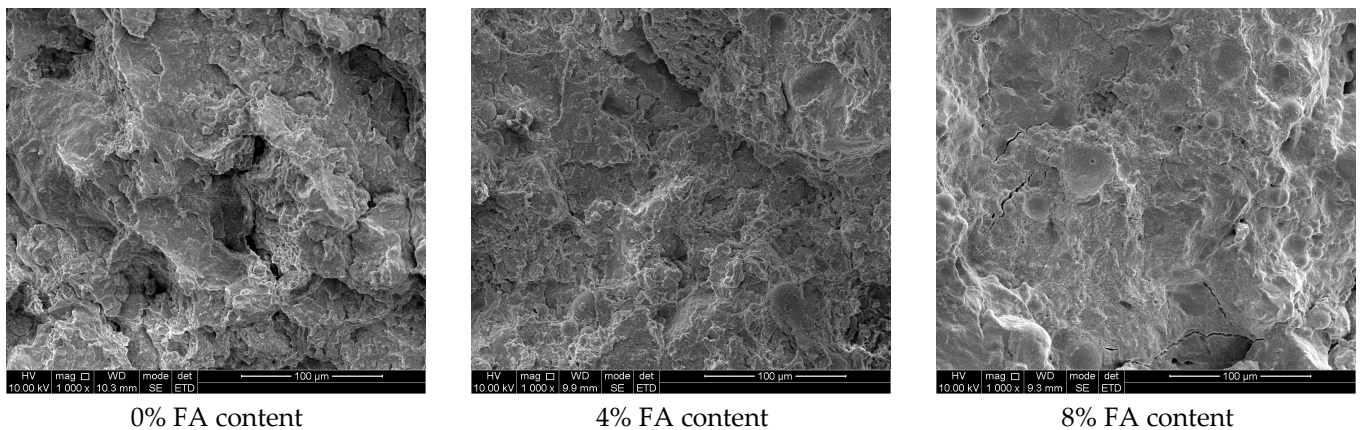


Figure 3. SEM images of the modified RC with different FA contents.

To compare the microscopic pore structure changes of the modified RC anti-seepage layer after RM leachate permeation, representative pure clay, 4%, and 8% FA-modified RC samples were examined using SEM before and after 60 days of permeation. The SEM images at a 10 µm scale are shown in Figure 4. As can be seen, the compacted modified RC particles were transformed from large lumps before permeation into many small particles, with their overall state changing from smooth and compact to rough and loose. Further, various small pores were generated in the modified RC after permeation. Compared to pure clay, the small clay particles of the FA-modified RC were significantly reduced, which was consistent with results reported by Zhao et al. [25].

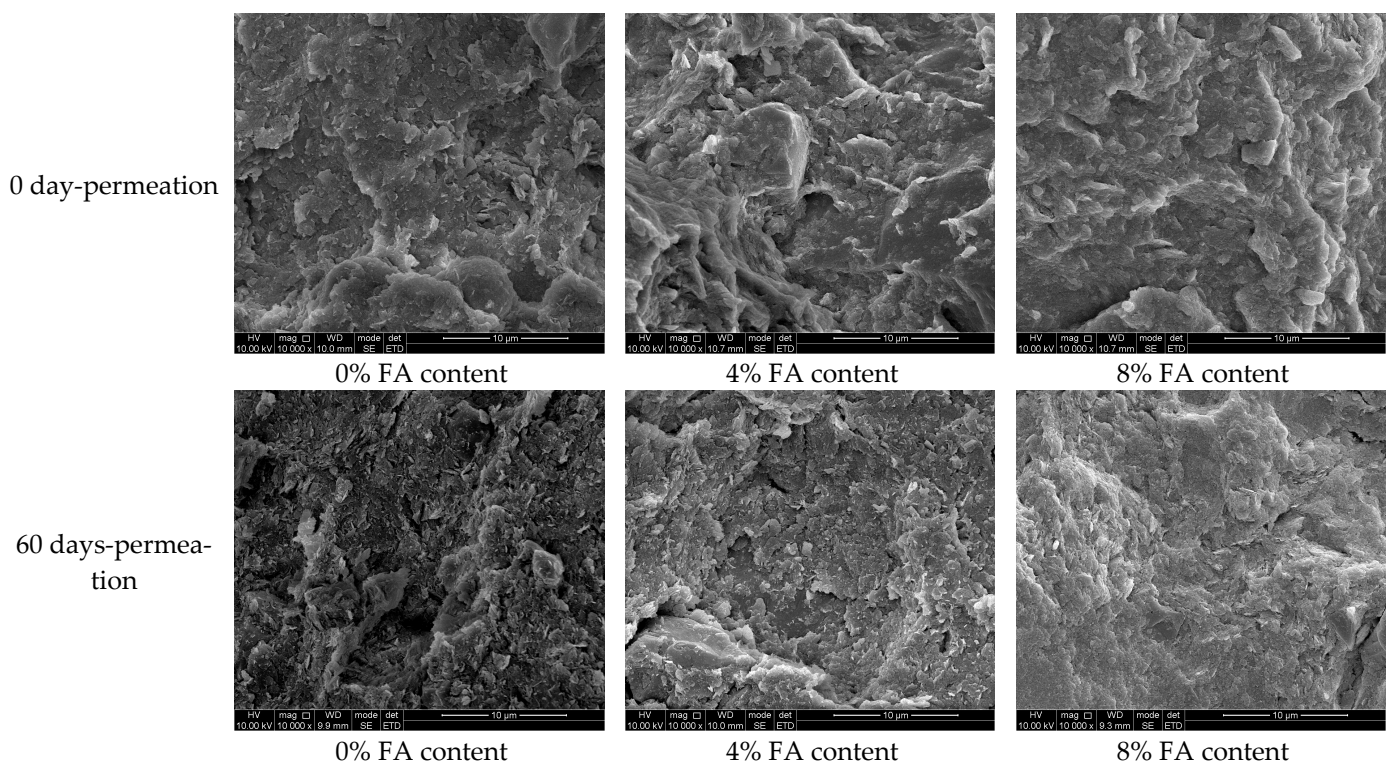


Figure 4. SEM images of modified RC before and after 60 days' permeability test.

3.2.2. Quantitative Analysis of Particle Changes

To facilitate the identification of particles and perform numerical statistical analyses, the contrast enhancement diagram, binarization diagram, and identification diagram of

compacted FA-modified RC before and after 60 days' permeation under RM leachate are shown in Figure 5.

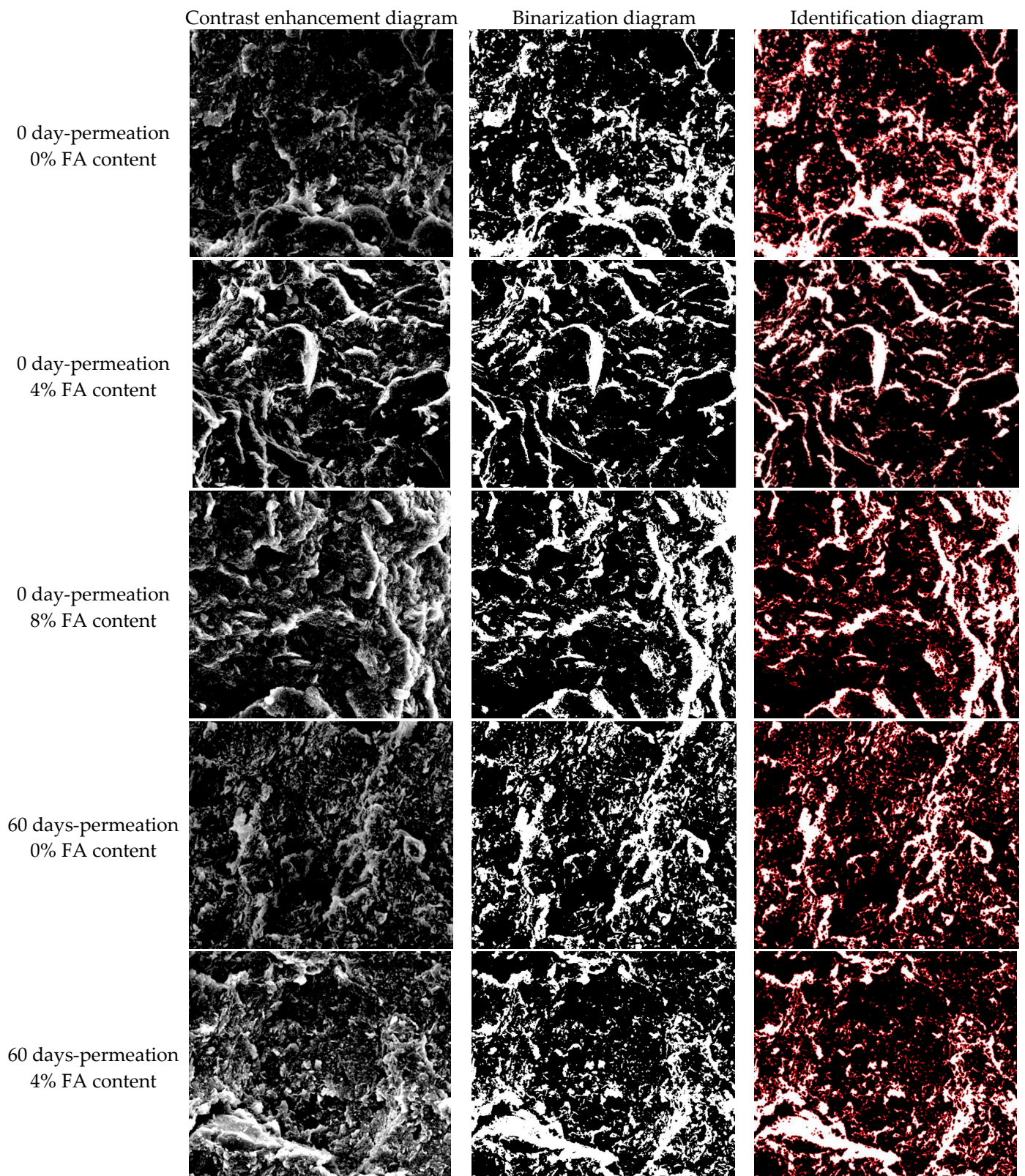


Figure 5. Cont.

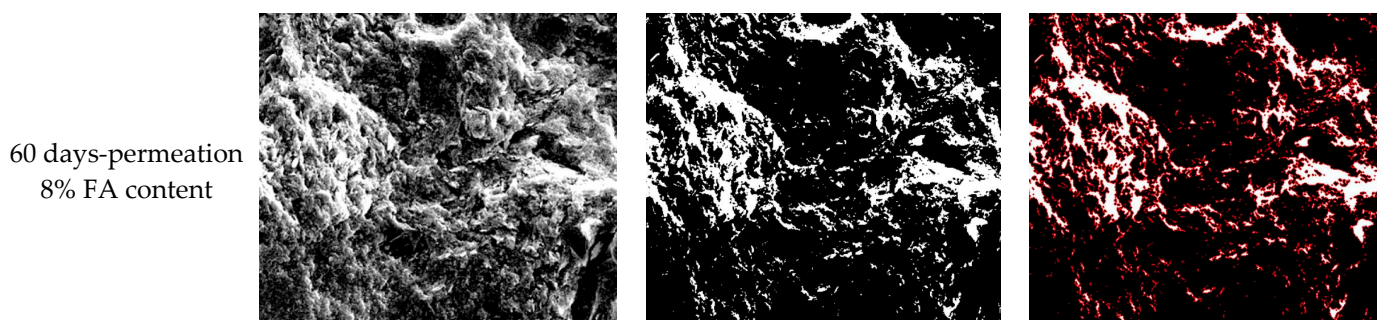


Figure 5. Digital processing technology for scanning electron microscope image.

Based on the recognition image, the changes in the size and quantity of clay particles in the scanning electron microscope image were calculated. The changes in the number, area, and average maximum radius of the particles before and after the permeation of RM leachate and under different FA contents are shown in Table 3.

Table 3. Electron microscope scanning image data obtained through digital processing.

Unit: Pixels	0 Day-Permeation			60 Days-Permeation		
	0%	4%	8%	0%	4%	8%
Image area	146,000	146,000	146,000	146,000	146,000	146,000
Number of particles	1127	928	1034	1542	1464	1372
Particle area	69,648	58,556	64,831	69,852	72,468	63,249
Maximum area of particles	10,959	12,697	15,212	6689	9837	7043
Average particle area	61.8	63.1	62.7	45.3	49.5	46.1
Maximum perimeter of particles	2675	2907	3379	1842	2441	2062
Average perimeter of particles	19.3	22.5	23.4	13.8	14.1	15.3
Maximum particle radius	199.7	180.2	247.6	151.4	184.1	161.1
Average maximum particle radius	3.1	3.5	3.8	2.5	2.7	2.6

Digitizing the micro electron microscope images reflected the changes in the micro pore particles of compacted FA-modified RC before and after the permeation of RM leachate. After the permeation of RM leachate, the overall number of modified RC particles significantly increased. Among them, pure RC particles with 0% FA content were the most, while the number of particles in 4% and 8% FA-modified RC was relatively smaller. The overall particle area did not change much before and after permeation, while the maximum and average particle areas of the particles significantly decreased after the permeation of RM leachate. The maximum perimeter and average circumference of the modified RC particles also decreased after the permeation, while the maximum radius and average maximum radius both decreased to varying degrees. After permeation, the original pore structure of the soil was destroyed, leading to the loss of soil particles, resulting in a loose pore structure, smaller particles, and more particulate matter [35,36]. However, with the addition of FA, the soil structure became more compact, and the degree of particle aggregation was higher, reducing the impact of RM leachate on the pore particles of the RC [37].

3.3. Effects of RM Leachate on Specific Surface Area of Modified RC

3.3.1. Comparative Analysis of Specific Surface Area

Figure 6 shows the comparison of surface area among different modified RCs. The lateral comparison of specific surface area showed that the 4% FA-modified RC sample had the largest specific surface area at the early stage of permeation, followed by those of pure clay and 8% FA-modified RC, which had the smallest specific surface area. Furthermore, in the intermediate and final stages of permeation, a larger FA content resulted in a higher specific surface area of the modified RC. FA is the product of pulverized coal combustion, with volcanic ash as the main chemical component and SiO_2 and Al_2O_3 as the main active

mineral components [38]. The activity of FA can be enhanced in alkaline environments, and incorporating FA and lime into RC can rapidly induce a short-term reactive effect and a long-term pozzolanic reaction [39]. Meanwhile, the SEM image showed that FA contained more than 70% of glass microbeads with a complete shape, smooth surface, and compact texture. However, after a period during which the low 4% FA-modified RC was kept in the initial non-permeation stage, it seemingly reacted with alkaline substances such as CaO in a humid environment through the activity effect, thereby generating gelling substances such as CSH and CAH and increasing the specific surface area of soil particles. In contrast, the large 8% FA-modified RC showed a large number of glass microbeads with a smooth surface and complete particle shape that led to an incomplete activation effect and pozzolanic reaction, which in turn resulted in a reduced specific surface area compared to the initial clay. After a series of pozzolanic reactions and activation effects in the intermediate and late stages of permeation, the RC samples with a higher FA content produced more gelling materials, leading to a higher specific surface area [40].

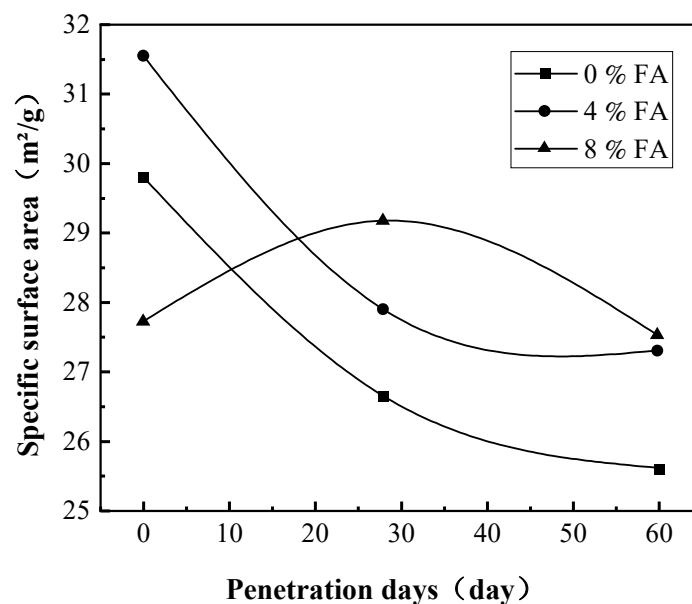


Figure 6. Comparison of surface area among different modified RCs.

3.3.2. Cause Analysis

As the permeation time increased, the specific surface area of the 8% FA-modified RC first increased and then decreased, increasing from 27.71 m²/g before permeation to 29.17 m²/g and then decreasing to 27.52 m²/g after 60 days. All other samples showed a decreasing trend in specific surface area. The 4% FA-modified RC decreased from 31.55 m²/g to 27.52 after 60 days of penetration. RM leachate is a highly alkaline and highly concentrated industrial wastewater with a large number of free alkaline anions, which can corrode soil structure and reduce soil strength, resulting in a decrease in soil specific surface area [41,42]. Therefore, the modified RCs all showed varying degrees of reduction in specific surface area with increasing days of permeation. As there was a large amount of FA that did not completely react in the 8% FA-modified RC, it reacted more completely in the alkaline and humid environment. The increase in specific surface area through the production of gelling substances can overcome the reduction in specific surface area caused by RM leachate-induced corrosion, resulting in an increase in specific surface area in the 8% FA-modified RC in the medium-term. However, as time increased, the corrosion caused by RM leachate to the structure became more severe, such that the specific surface area eventually decreased [43].

3.4. Effects of RM Leachate on Modified RC Pore Structure

3.4.1. Adsorption Characteristics of Modified RC

To investigate the change of pore structure of the compacted modified RC affected by RM leachate and explain the effect of RM leachate on the modified RC anti-seepage layer at a microscopic scale, the adsorption capacity is evaluated by comparing the isothermal adsorption curves of modified RC under varied conditions. Furthermore, based on the type of the adsorption isothermal curves and the major hysteresis loops, the overall morphology of the pore structure of modified RC can be roughly determined.

The adsorption curves of different FA-modified RCs are shown together in Figure 7. At 60 days of penetration, the adsorption capacity of the sample with a 0% FA addition was $77.62 \text{ cm}^3/\text{g}$, while the sample with a 4% FA addition was $71.35 \text{ cm}^3/\text{g}$. The adsorption capacity of the sample with an 8% FA addition was the lowest, which was at $64.78 \text{ cm}^3/\text{g}$. As the FA content increased, the adsorption of the modified RC gradually decreased, presumably owing to the many glass microbeads with a smooth surface contained in the FA. Although some of these beads can gelatinize with the clay to form a stable structure, much of the FA is not involved in such interaction, as these glass beads reduce the adsorption capacity of the modified RC [44,45].

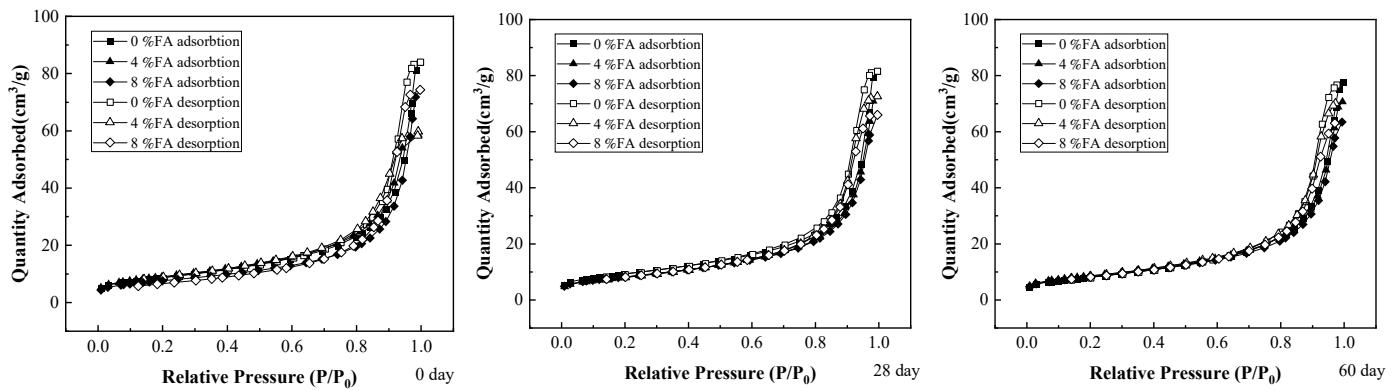


Figure 7. Adsorption curves of modified RC with varying FA contents.

Figure 8 shows the adsorption curves of the modified RC with the same FA content as a function of permeation time. In this case, the maximum adsorption capacity of all modified RCs all decreased with increasing permeation time. This was attributed to the clay particles becoming loose after leachate corrosion, which further damaged the clay pore structure and weakened the adsorption capacity, thereby resulting in the reduction of the maximum adsorption capacity.

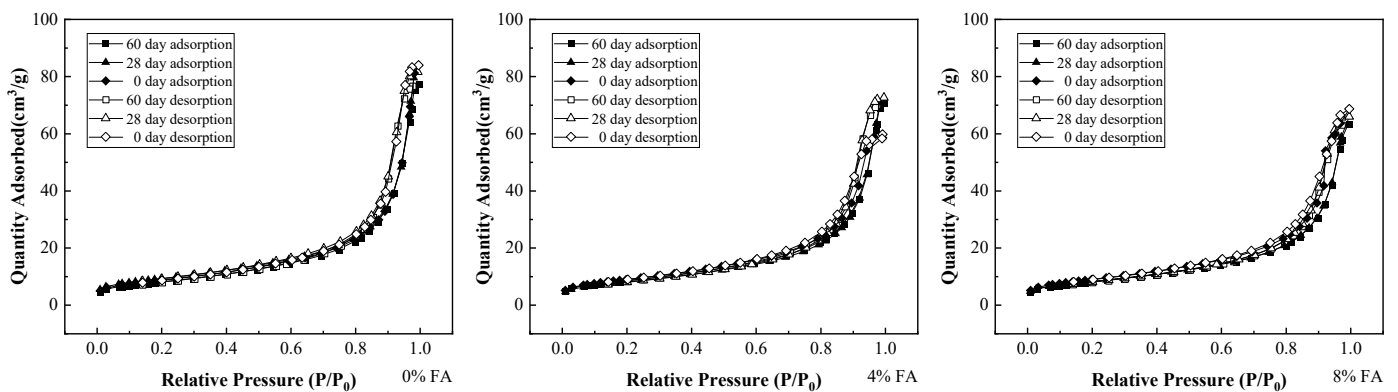


Figure 8. Adsorption curves of modified RC with the same FA content at different permeation times.

In summary, the type of isotherm curve of the modified RC with different FA contents did not change with increasing content or corrosion, and the types were all classified as type IV isotherms. The approximate hysteresis loop types of the RC with the same FA content were also unchanged and belonged to the H3 type of isotherm, indicating that neither the corrosion of the RM leachate nor FA modification had any effect on the isothermal adsorption curves or the hysteresis loop type of the RC.

3.4.2. Pore Size Distribution of Modified RC

The BET pore analyzer can determine the pore distribution of an object and reveal any changes in soil pore size distribution with the permeation and corrosion of RM leachate through exploring the pore size-distribution law of RC. According to the IUPAC classification, porous substances can be defined as macroporous when the pore size is larger than 50 nm, mesoporous when the pore size ranges between 2 and 50 nm, and microporous when the pore size is less than 2 nm.

Figure 9 shows the variation in pore size in all modified RC types as a function of FA contents under the same permeation time. The pore size of the modified RC particles was dominated by micropores and mesopores 1–2 and 2–50 nm in size, respectively. Furthermore, the pore size distribution showed a single-shouldered peak, approximately 0.25 dV/dr, with the 2–8 nm pore size accounting for the dominant proportion. Before permeation, this single-shouldered peak was highest for pure RC and lowest for the 8% FA-modified RC; specifically, the pore size distribution decreased sequentially in 0%, 4%, and 8% FA-modified RC for pore size intervals greater than 8 nm. After 28 days of permeation, the pore size distribution remained as a single-shouldered peak with no large variation in height and a pore size distribution of 2–8 nm. However, after 60 days of permeation, the signal-shouldered peaks of different FA-modified RCs progressively increased, with the overall pore size distribution consistent with what they were before permeation. As a result, the pore size distribution of the modified RC was inversely proportional to the FA content. Due to a certain period of incubation before permeation, the clay was combined with and reacted with FA to produce CSH and CAH, which filled the voids between the soil particles, resulting in a change in pore size, whereby the pore-size distribution of the modified clay was slightly lower than that of pure clay [40,41]. A considerable number of alkaline ions entered the soil during the permeation process of RM leachate, generating an alkaline environment. However, it had a negligible impact on the pozzolanic reaction of FA. As such, although the overall pore-size distribution produced minor changes, it still decreased sequentially with 0%, 4%, and 8% FA-modified RC.

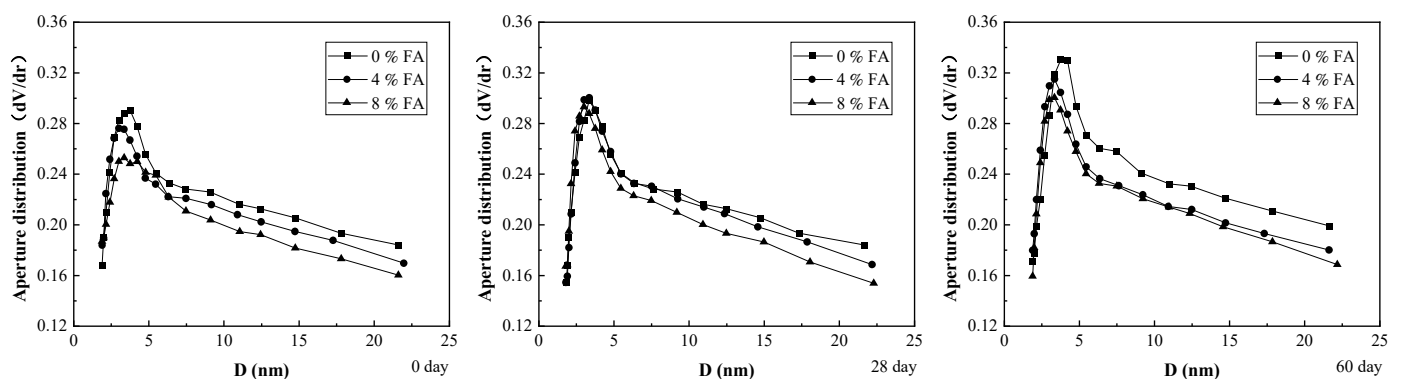


Figure 9. Pore size distribution of modified RC with different FA contents under the same permeation time.

The variation in pore size distribution with permeation time for the modified RC with the same FA content is shown in Figure 10. Under the corrosion of RM leachate, the single-shouldered peak became higher, and the pore size increased with permeation time for all modified RCs with the same FA content. After 60 days of permeation, the single-shoulder

peak of the modified RC with 8% FA content was still the lowest at about 0.30 dV/dr, and the pore size was relatively small compared to other samples. The high amount of NaOH, NaHCO₃, NaAl(OH)₄ and other free bases contained in RM leachate formed many free alkaline anions when dissolved in the liquid phase, destroying the original pore structure of the soil and causing the loss of soil particles [17]. As a result, the pore size distribution increased to varying degrees, and the peak pore size of the concentrated distribution of the single-shouldered peak became larger. The produced CSH and CAH from the slow pozzolanic reaction of the FA-modified RC reduced the damage of RM leachate to the soil structure to a certain extent [46]. Therefore, the pore size distribution pattern indicated that as permeation time increased, the single-shouldered peak of pure clay increased more than the peaks for the FA-modified RC.

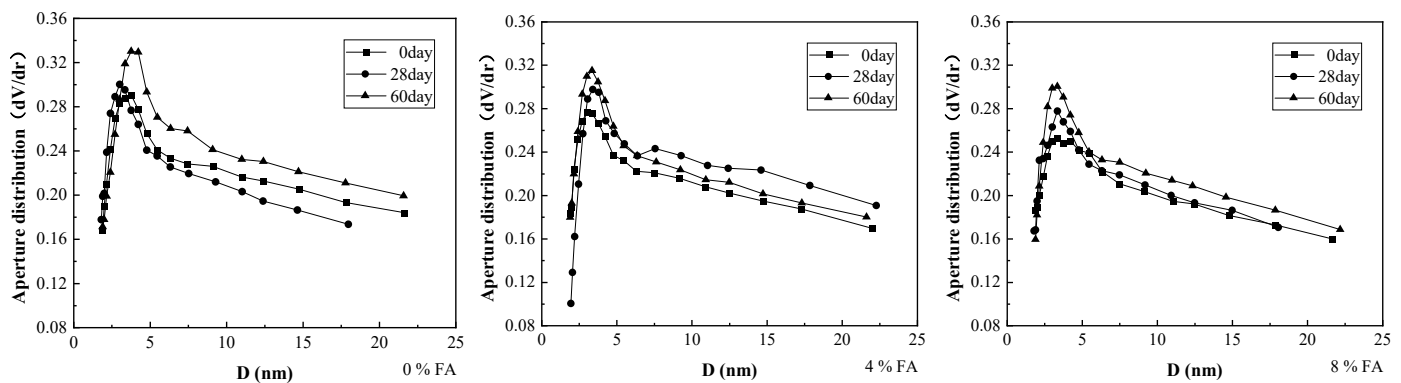


Figure 10. Pore size distribution of modified RC with the same FA content under different permeation times.

4. Conclusions

In this study, we performed the permeability test on FA-modified RC samples using a flexible wall permeameter. The changes in the particle surface of FA-modified RC were analyzed before and after the test using SEM technology. The gas adsorption method was used to determine the specific surface area of the FA-modified RC. After analyzing the adsorption changes in the modified RC caused by the leachate, we arrived at the following conclusions:

- (1) In the early stage of RM leachate permeation, the permeability coefficient of the modified RC gradually increased with increasing FA content. Further, as permeation time increased, the permeability coefficient of compacted modified RC varied with the content of FA. The permeability coefficient of modified RC with 8% FA content showed a significant decreasing trend, reaching 5.98×10^{-11} m/s after stabilization, being significantly affected by permeation but with enhanced anti-seepage ability.
- (2) The permeation of RM leachate led to the destruction of the original pore structure of the clay soil at the microscopic level. Specifically, the particle block became smaller, the amount of the particle matter increased, and the specific surface area decreased. The modified RC sample with an 8% FA content showed a phenomenon of first increasing and then decreasing in specific surface area, overall decreasing from 27.71 m²/g before permeation to 27.52 m²/g, with little change. This indicates that the specific surface area of this sample was not significantly affected by penetration, exhibiting stronger stability.
- (3) An increased FA content makes the soil structure more compact at the microscopic level, presenting particle aggregation, increased specific surface, a small pore-size distribution, and a decreased height of the single-shouldered peak. After 60 days of permeation, the single-shouldered peak of the modified RC with an 8% FA content was still the lowest at about 0.30 dV/dr. Compared to other samples, the pore size was smaller and less affected by the leachate.

Overall, the microstructure of modified RC with an 8% FA content is less affected by leachate. In the following study, a further analysis will be conducted on the adsorption capacity of the FA content sample for heavy metals, and its potential engineering application will be evaluated based on its engineering mechanical properties.

Author Contributions: Conceptualization, Y.Z.; methodology, Y.Z., Y.W. and Y.Y.; validation, H.H.; formal analysis, Y.W., Y.Y. and H.H.; investigation, Y.Z. and D.P.; resources, Y.Z.; data curation, Y.Y., H.H. and H.Q.; writing—original draft preparation, Y.Z. and Y.W.; writing—review and editing, Y.Z., Y.W. and D.P.; visualization, Y.W. and H.Q.; supervision, Y.Z.; project administration, Y.Z.; funding acquisition, Y.Z. All authors have read and agreed to the published version of the manuscript.

Funding: This research is funded by Natural Science Foundation of Sichuan, China, grant number 2022NSFSC0240.

Institutional Review Board Statement: Not applicable.

Informed Consent Statement: Not applicable.

Data Availability Statement: The data are available upon reasonable request from the corresponding author.

Conflicts of Interest: The authors declare no conflict of interest.

References

- Xu, D.; Zhan, C.; Liu, H.; Lin, H. A critical review on environmental implications, recycling strategies, and ecological remediation for mine tailings. *Env. Sci. Pollut. Res. Int.* **2019**, *26*, 35657–35669. [CrossRef]
- Xinkuan, L.; Jianxiong, K. Status and Measures of preventing and controlling environmental risks in tailing impoundment. *IOP Conf. Ser. Earth Environ. Sci.* **2021**, *10*, 1755–1315. [CrossRef]
- Miao, Z.; Yan, C.; Liu, L.; Ren, L.; Chen, Y. Prevention of metal tailings based on ecological safety. *IOP Conf. Ser. Earth Environ. Sci.* **2020**, *558*, 042027. [CrossRef]
- Cheng, L.; Zhu, S. Study on Comprehensively utilizing tailings at home and abroad. *China Resour. Compr. Util.* **2005**, 30–32.
- Narayanan, R.P.; Palantavida, S. An initial screening of commercial phosphorus ligands on the recovery of metal ions from red mud. *Mater. Today Proc.* **2021**, *41*, 692–697. [CrossRef]
- Feedback Inspection Report of the Fourth Central Ecological and Environmental Protection Supervision Group. Available online: https://www.mee.gov.cn/xxgk2018/xxgk/xxgk15/202102/t20210201_819655_wh.html (accessed on 1 February 2021).
- Mei, G.; Wang, Y. Statistic analysis and countermeasure study on tailings pond accidents in China. *J. Saf. Sci. Technol.* **2010**, *6*, 211–213.
- Yang, H.; Bai, B.; Nie, Q. Experimental study of influence of red mud leachate on cohesive soil and reinforced red mud. *Rock Soil Mech.* **2017**, *38*, 299–304.
- Ghanbarian, B. Modeling Physical and Hydraulic Properties of Disordered Porous Media: Applications from Percolation Theory and Fractal Geometry. Ph.D. Thesis, Wright State University, Dayton, OH, USA, 2014.
- Hunt, A.G.; Ghanbarian, B.; Saville, K.C. Unsaturated hydraulic conductivity modeling for porous media with two fractal regimes. *Geoderma* **2013**, *207*, 268–278. [CrossRef]
- Benson, C.H.; Zhai, H.; Wang, X. Estimating hydraulic conductivity of compacted clay liners. *J. Geotech. Eng.* **1995**, *121*, 366–387. [CrossRef]
- Sophia, A.; Swaminathan, K. Assessment of the mechanical stability and chemical leachability of immobilized electroplating waste. *Chemosphere* **2005**, *58*, 75–82. [CrossRef]
- Paramasivam, S.; Sajwan, K.S.; Alva, A.K.; Adriano, D.C.; Punshon, T.; van Clief, D.; Hostler, K.H. Comparative study of elemental transport and distribution in soils amended with fly ash and sewage sludge ash. *Chem. Trace Elem. Fly Ash* **2003**, 189–202.
- Jeyaseelan, S.; Qing, L.G. Development of adsorbent/catalyst from municipal wastewater sludge—ScienceDirect. *Water Sci.* **1996**, *34*, 499–505. [CrossRef]
- Zhang, H.; Sun, L.; Sun, T. Solubility of trace elements and heavy metals from stabilized sewage sludge by fly ash. *Bull. Env. Contam. Toxicol.* **2009**, *83*, 752–756.
- Metelková, Z.; Boháč, J.; Sedlářová, I.; Příkryl, R. Changes of pore size and of hydraulic conductivity by adding lime in compacting clay liners. In *Geotechnical Engineering: New Horizons*; IOS Press: Amsterdam, The Netherlands, 2011.
- Li, J.S.; Xue, Q.; Wang, P.; Liu, L. Influence of leachate pollution on mechanical properties of compacted clay: A case study on behaviors and mechanisms. *Eng. Geol.* **2013**, *167*, 128–133. [CrossRef]
- He, J.; Wang, Y.; Li, Y.; Ruan, X. Effects of leachate infiltration and desiccation cracks on hydraulic conductivity of compacted clay. *Water Sci. Eng.* **2015**, *8*, 151–157. [CrossRef]
- Li, Y.; Cleall, P.J. Analytical solutions for advective–dispersive solute transport in double-layered finite porous media. *Int. J. Numer.* **2012**, *36*, 438–460. [CrossRef]

20. Barone, F.S.; Yanful, E.K.; Quigley, R.M.; Rowe, R.K. Effect of multiple contaminant migration on diffusion and adsorption of some domestic waste contaminants in a natural clayey soil. *Can. Geotech. J.* **1989**, *26*, 189–198. [[CrossRef](#)]
21. Oztoprak, S.; Pisirici, B. Effects of micro structure changes on the macro behaviour of Istanbul (Turkey) clays exposed to landfill leachate. *Eng. Geol.* **2011**, *121*, 110–122. [[CrossRef](#)]
22. Guo, Y.; Cao, L.; Feng, X.; Liu, H. Influence of leachate on properties and regions of compacted clay layer: A column experiment. *Soil Sediment Contam. Int. J.* **2019**, *28*, 684–694. [[CrossRef](#)]
23. Ural, N. The significance of scanning electron microscopy (SEM) analysis on the microstructure of improved clay: An overview. *Open Geosci.* **2021**, *13*, 197–218. [[CrossRef](#)]
24. Zhang, Q.; Lu, H.; Cai, G.; Dong, Y.; Wang, W. Adsorption and transportation properties of cadmium in modified clay containing sewage sludge ash as landfill liner. *J. Southeast Univ.* **2016**, *46*, 174–178.
25. Zhao, Y.; Xue, Q.; Huang, F.; Hu, X.; Li, J. Experimental study on the microstructure and mechanical behaviors of leachate-polluted compacted clay. *Environ. Earth Sci.* **2016**, *75*, 1006. [[CrossRef](#)]
26. Zhang, Y.; Yu, Y.; Qin, H.; Peng, D.; Chen, X. Dynamic adsorption characteristics of Cr(VI) in red-mud leachate onto a red clay anti-seepage layer. *Toxics* **2022**, *10*, 606. [[CrossRef](#)]
27. Bardestani, R.; Patience, G.S.; Kaliaguine, S. Experimental methods in chemical engineering: Specific surface area and pore size distribution measurements—BET, BJH, and DFT. *Can. J. Chem. Eng.* **2019**, *97*, 2781–2791. [[CrossRef](#)]
28. Brunauer, S.; Emmett, P.H.; Teller, E. Adsorption of Gases in Multimolecular Layers. *J. Am. Chem. Soc.* **1938**, *60*, 309–319. [[CrossRef](#)]
29. Fu, X.; Du, Y.; You, X.; Yang, Y.; Jiang, Z. Influences of red mud leachates on hydraulic performance of a modified geosynthetic clay liner. *Chin. J. Geotech. Eng.* **2021**, *43*, 706–714.
30. Cheshomi, A.; Eshaghi, A.; Hassanpour, J. Effect of lime and fly ash on swelling percentage and Atterberg limits of sulfate-bearing clay. *Appl. Clay Sci.* **2017**, *135*, 190–198. [[CrossRef](#)]
31. Mishchuk, N.A.; Marinin, A.I.; Marchenko, A.M. Coagulation, sedimentation, and consolidation of aqueous clay dispersions. *J. Water Chem. Technol.* **2020**, *42*, 8–15. [[CrossRef](#)]
32. Wang, Y.; Liu, X.; Li, Y.; Li, D.; Zhang, W.; Xue, Y. Tailings after iron extraction in bayer red mud by biomass reduction: Pozzolanic activity and hydration characteristics. *Materials* **2021**, *14*, 3955. [[CrossRef](#)]
33. Yue, B.; Zhao, Z.; Qian, Z. Influence of five additives on no loading swelling potential of red clay. *Appl. Sci.* **2022**, *12*, 3455. [[CrossRef](#)]
34. Kwan, A.K.H.; Li, Y. Effects of fly ash microsphere on rheology, adhesiveness and strength of mortar. *Constr. Build. Mater* **2013**, *42*, 137–145. [[CrossRef](#)]
35. Yu, X.; Shi, W.; Wang, X.; Liang, F.; Xu, W. Simulation on mesoscopic deformation and failure mechanism of dissolved rock mass using digital image processing technology. *Carsologica Sin.* **2020**, *39*, 409–416.
36. Wang, Q.; Chen, J.; Liu, J.; Yu, M.; Geng, W.; Wang, P.; Wu, Z. Relationships between shear strength parameters and microstructure of alkaline-contaminated red clay. *Environ. Sci. Pollut. Res.* **2020**, *27*, 33848–33862. [[CrossRef](#)] [[PubMed](#)]
37. Norouzi, A.; Uygur, E.; Nalbantoglu, Z. A review on the effects of landfill leachate on the physical and mechanical properties of compacted clay liners for municipality landfills. *Arab. J. Geosci.* **2022**, *15*, 1174. [[CrossRef](#)]
38. Astuti, W.; Chafidz, A.; Wahyuni, E.T.; Prasetya, A.; Bendiyasa, I.M.; Abasaed, A.E. Methyl violet dye removal using coal fly ash (CFA) as a dual sites adsorbent. *J. Environ. Chem. Eng.* **2019**, *7*, 103262. [[CrossRef](#)]
39. Okeke, C.; Abbey, S.; Oti, J.; Eyo, E.; Johnson, A.; Ngambi, S.; Abam, T.; Ujile, M. Appropriate use of lime in the study of the physicochemical behaviour of stabilised lateritic soil under continuous water ingress. *Sustainability* **2020**, *13*, 257. [[CrossRef](#)]
40. Tang, H.; Yang, Z.; Zhu, H.; Dong, H. Experimental study on the mechanical properties of Xinyang red clay improved by lime and fly ash. *Appl. Sci.* **2023**, *13*, 6271. [[CrossRef](#)]
41. Nie, Q.; Li, Y.; Wang, G.; Bai, B. Physicochemical and microstructural properties of red muds under acidic and alkaline conditions. *Appl. Sci.* **2020**, *10*, 2993. [[CrossRef](#)]
42. Li, X.; Guo, Y.; Zhu, F.; Huang, L.; Hartley, W.; Li, Y.; Kong, X.; Xue, S. Alkalinity stabilization behavior of bauxite residue: Ca-driving regulation characteristics of gypsum. *J. Cent. South Univ.* **2019**, *26*, 383–392. [[CrossRef](#)]
43. Wang, Z.; Wang, D.; Ji, P.; Cheng, X. Study on the formation of microglass beads during staged combustion. *Energy Fuels* **2018**, *32*, 8069–8077. [[CrossRef](#)]
44. Andavan, S.; Pagadala, V.K. A study on soil stabilization by addition of fly ash and lime. *Mater. Today Proc.* **2020**, *22*, 1125–1129. [[CrossRef](#)]
45. Amiralian, S.; Chegenizadeh, A.; Nikraz, H. A review on the lime and fly ash application in soil stabilization. *Int. J. Biol. Ecol. Environ. Sci.* **2012**, *1*, 124–126.
46. Liu, Z.K.; Guo, T.; Wang, J. Effect of the fly ash lime fly ash on the mechanical properties of red clay in Guilin. *Hydrogeol. Eng. Geol.* **2017**, *44*, 86–92.

Disclaimer/Publisher’s Note: The statements, opinions and data contained in all publications are solely those of the individual author(s) and contributor(s) and not of MDPI and/or the editor(s). MDPI and/or the editor(s) disclaim responsibility for any injury to people or property resulting from any ideas, methods, instructions or products referred to in the content.